Unraveling electrokinetics – a brand new and innovative workflow for the quantification of electrokinetic properties of siliciclastic rocks

Matthias Halisch[1,*], *Stephan* Kaufhold[2], and *Christian* Weber[2]

[1]Leibniz Institute for Applied Geophysics (LIAG), Dept. 5 Petrophysics & Borehole Geophysics, 30655 Hannover, Germany
[2]Federal Institute for Geosciences and Natural Resources (BGR), Dept. B2.1 Technical Mineralogy, 30655 Hannover, Germany

Abstract. Electrokinetic properties have been measured, assessed and quantified for a very long time, mostly for classic colloidal systems (e.g., soils) or suspensions (e.g., clay-water-mixtures). Electrokinetic effects are used for both, fundamental investigations, such as the quantification of quadrature electrical conductivity and polarization processes, as well as for applied research, such as the systematic investigation of fluid stabilities (e.g. of solvents and proppants). Nevertheless, the quantification of electrokinetic parameters is extremely challenging. First, because they cannot be measured directly. Common techniques utilize the measurement of electrokinetic effects, which can be transferred to distinct electrokinetic parameters. Second, because electrokinetic properties depend on a high number of material and fluid quantities, such as the type of mineral and fluid phase, grain size, grain shape, grain roughness, ion content of the fluid, ion valence, ion mobility and pH-value. Although it is possible to quantify these properties on a general base for different formation, they can differ widely within natural rocks. Furthermore, specimen need to be crushed for the analysis. By doing this, the in-situ grain geometry and surface topology is destroyed. Even worse, milling causes the occurrence of amorphous mineral phases, which are mineralogical equivalent to the originating phases, but which may greatly differ in terms of electrokinetic properties. Hence, the value of the so derived data is very questionable. Within this case study, we will present a brand new and highly innovative methodical approach to overcome the issues as mentioned before. We will present and discuss both, very first electrokinetic data from a variety of siliciclastic rocks that have been processed as described in this manuscript, as well as the sample processing workflow.

1 Key Motivation

The key motivation for this innovative and new workflow lies within the fundamental research and understanding of the so-called “Induced Polarization effect” that was observed and published for the first time in 1920 by Conrad Schlumberger. Originally developed for prospecting ore deposits, the Induced Polarization (IP) or Spectral Induced Polarization (SIP) method is used to characterize natural solid and unconsolidated rocks, by covering many different approaches. Possibly more than any other geophysical method, SIP is able to build an important bridge between field and laboratory scale, i.e. between application and process and fundamental research [e.g., 1-6]. The main interest of basic research here is to comprehensively describe or characterize the causes of the IP effect in sedimentary rocks. In addition to investigating empirical correlations between SIP related parameters and classical petrophysical properties, such as specific surface area [e.g., 7], or permeability [e.g., 2], recent research has also focused on understanding the physical and electrochemical interaction between the rock-forming matrix and the fluid-filled pore space [e.g., 8, 9]. Based on this, varieties of models have been developed in recent years to describe the IP effect phenomenological. In this context, these models are either grain-based [e.g., 10-13], or pore-space based [e.g., 14-17] and take into account, at least to some extent, corresponding characteristic geometric structures and sizes found at the pore scale.

1.1 IP-theory

If an external electric field E is applied, a current density (j) is formed in any material, which is composed of a conduction current (j_L) and a displacement current (j_V):

$$j = j_L + j_V. \qquad (1)$$

The conduction current density is obtained directly from Ohm's law:

$$j_L = \sigma E, \qquad (2)$$

where σ corresponds to the electrical conductivity of the material. Now, if - as is the case with SIP - a periodic alternating electric field is present (i.e., $E \sim \exp(i\omega t)$, with

* Corresponding author: matthias.halisch@leibniz-liag.de

$i = \sqrt{-1}$, ω = angular frequency = $2\ \pi\ f$, t = time), the displacement current density is given by:

$$j_V = d/dt\ \varepsilon\ E = i\omega\ \varepsilon\ E. \qquad (3)$$

The ε here corresponds to the so-called dielectric constant and is composed of the relative dielectric constant and the vacuum dielectric constant ($\varepsilon = \varepsilon_r\ \varepsilon_0$). If we now consider the low, i.e., the SIP-typical frequency range (~ 1 mHz to ~ 10 kHz), the ratio of conduction to displacement current density becomes very large, i.e., the displacement current density - and thus the influence of the dielectric constant of the material - becomes negligible [18]:

$$|j_L| / |j_V| = \sigma / (\varepsilon_r\ \varepsilon_0\ \omega) >> 1. \quad (4)$$

Consequently, the electrical material behaviour in this frequency range is dominated by the conductivity, which is described as a frequency-dependent and, in the case of inhomogeneous, natural rocks, moreover as a complex quantity consisting of real (σ') and imaginary part (σ'') [19]:

$$\sigma(\omega) = \sigma'(\omega) + i\sigma''(\omega). \qquad (5)$$

Due to different polarization mechanisms, there is a characteristic phase shift between the current and voltage signal by an angle φ:

$$\varphi(\omega) = \arctan\ (\sigma''\ (\omega) / \sigma'(\omega)). \qquad (6)$$

This measurable phenomenon is commonly referred to as the "IP effect". As listed in the introduction, quite a few variants and variations of phenomenological models (some mineral grain-based, others pore space-based) exist to describe, characterize, and reproduce the IP effect in a material-dependent, i.e., rock-specific, manner under ideal circumstances. The latter, however, is particularly challenging because, although there are recognized polarization mechanisms, their individual influence, integrated over the entire sample volume under investigation, is largely not understood. It is undisputed that the electrical conductivity ($\sigma(\omega)$) of a rock whose pore space is filled with electrolyte is largely determined by the electrical conductivity of the fluid (σ_w). That is, the rock-forming minerals behave relatively as "quasi-insulators" due to their very low electrical conductivity. However, electrochemical interactions cause the formation of a so-called interfacial conductivity ($\sigma_g(\omega)$) at the interface between the pore fluid and the rock matrix. Since this conductivity is also a complex quantity, the rock conductivity can be described using the so-called formation resistance factor F [20] as follows [21, 22]:

$$\sigma(\omega) = (\sigma w / F) + \sigma g'(\omega) + i * \sigma g''(\omega) \qquad (7).$$

Electrochemical processes and interactions result in a solid accumulation of ions on the surface of the mineral grain. This "solid" layer is called the Stern layer (or Helmholtz layer). The transition to the (free) pore fluid is formed by a region of diffusely distributed ions. The ion concentration within this diffuse laver decreases exponentially with distance from the Stern layer. Together, this results in the so-called electric double layer (EDL, Figure 1). As it can be seen from (7), the imaginary part of the rock conductivity (quadrature conductivity, also denoted as σ'') is caused solely by the contribution of the interfacial conductivity. Hence, the EDL occupies a central role in research on the IP effect, which is expressed in particular in the mechanistic models for the so-called membrane and Stern layer polarization. In these models, cations from the electrolyte accumulate firmly and diffusely on the usually negatively charged mineral surface: an EDL is formed. If an external alternating electric field is now applied, charge accumulation occurs and consequently a concentration gradient in the ion distribution. This concentration gradient is dissipated by diffusion after the electric field is switched off [23].

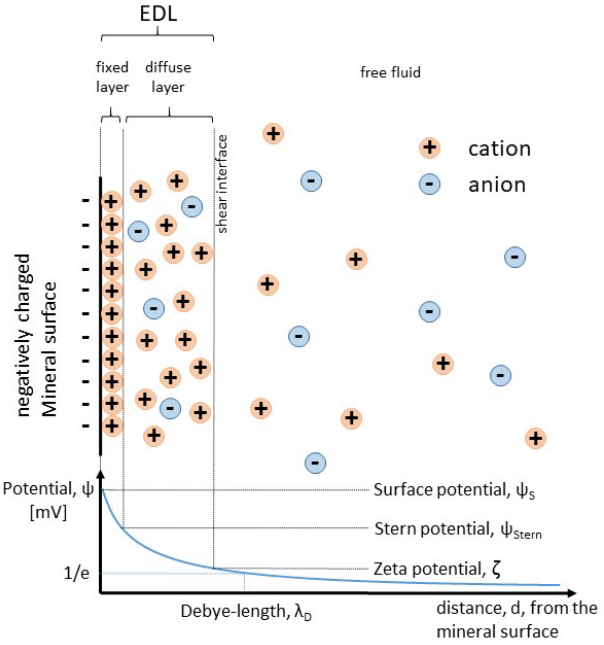

Fig. 1. Schematic representation of the charge carrier distribution at the interface between mineral grain (left) and electrolyte (right) without an externally applied electric field. At the negatively charged mineral surface (e.g., quartz) a fixed and a diffuse layer are formed, which together form the electrical double layer (EDL). The resulting potentials are shown in the lower part.

In addition to the dependence on the specific material surface, the research approaches based on the membrane polarization model focus primarily on the geometry or on the topology of the pore spaces, e.g. their diameter, their length, or their ratio to each other. Particularly noteworthy are the approaches to model membrane polarization by [24-28]. In addition, a few publications exist that attempt to include the influence of the electrical double layer in a highly generalized manner [e.g., 12, 29-31]. Nevertheless, all of these approaches lack systematically measured and validated, "in-situ" double-layer parameters of natural rocks and minerals. Closing this knowledge gap within the framework of this project is a key motivation.

1.2 Electrical double layer model

It is remarkable to note that research on the electrical double layer as well as on the IP effect has been carried out in parallel for almost a century, but that rudimentary efforts to link both research areas have only been made in the last 10 years. The characterization of the EDL has long been part of the standard repertoire in the fields of physical and inorganic chemistry as well as soil science and (clay) mineralogy, to name just a few of the disciplines with which rock physics or IP research could be synergistically linked. Comprehensive information on the formation, the dynamics, processes and applications around the EDL can be found in seminal textbooks [32, 33, 34].

However, crucial and linking for IP-related research on natural solid rocks is the formation of an EDL, so that when an external electric field is applied, the anions and cations in the diffuse layer as well as in the free fluid (cf. Fig.1) start to move according to the respective field direction. This leads to an accumulation of charge or to a "polarization effect" (Fig. 2), which in turn can be measured and interpreted as a contribution of the interfacial conductivity to the rock conductivity. The EDL is decisively characterized by the diffuse layer, i.e., as the dynamic part of itself.

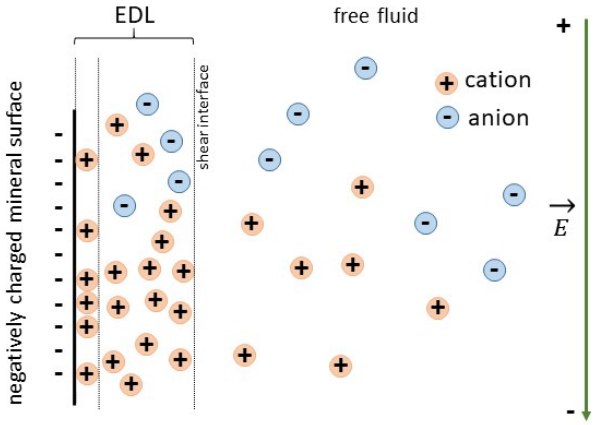

Fig. 2. Schematic representation of charge separation / accumulation with applied external alternating electric field (E). The EDL plays a decisive role for the polarization behaviour or for the IP effect.

The relevant parameter characterizing the diffuse part of the EDL is the so-called zeta potential [35, 36]. The zeta potential is defined as the electric potential at the shear layer of a moving particle in a suspension. Consequently, the zeta potential is an interfacial property (here at the solid-liquid interface) and depends on the surface potential (or surface charge) and thus on the mineral, its surface, and the properties of the electrolyte (see Table 1) [34]. In conclusion, there is a direct relationship between the interfacial conductivity (eq. 7) and the zeta potential. Moreover, the zeta potential is a main indicator of the electrostatic repulsion of ions in the dispersion medium, i.e., the higher the zeta potential, the greater the repulsion, i.e., the less likely is agglomeration of small charged (mineral) particles. In classical EDL research, this relationship is used to characterize the stability of colloidal dispersions [37]. However, a look at the relevant EDL-related literature also shows that for decades almost exclusively only so-called colloidal systems have been the focus of research interest [e.g., 34, 35, 38-40].

Table 1. Summary of relevant dependencies of the zeta potential of solid and liquid phase.

solid phase (mineral)	liquid phase (electrolyte)
type of mineral	valency
surface	ion mobility
roughness	ion concentration
grain form	ph-value
grain size	temperature

A classical colloidal system consists of particularly finely dispersed, especially small (sub-micrometer range) particles (e.g. clay particles), which are contained in a dispersion medium. Thus, two main questions arise for SIP-related EDL characterization of natural solid rocks:

1.) How can the zeta potential be determined on a solid rock, taking into account the multiple dependencies as listed in Table 1?
2.) Does the necessary technology for the preparation and for the measurement exist at all?

2 Electrokinetic methods

In the course of our own preliminary work, we have investigated precisely these two questions. In order to be able to answer the first question, we will first take a brief look at the existing measurement methods. A variety of measurement techniques exist for determining the zeta potential, all of which are based on the measurement of an electrokinetic effect [36]. EDL properties themselves (as shown in Fig.1.) cannot be measured directly. One talks about an electrokinetic effect if the coupling of a mechanical and an electrical force is present in any combination. The only important thing is that two phases (here: solid-liquid) move relative to each other. In practice, one phase is moving while the other remains stationary.

Table 2 summarizes the main measurement techniques of electrokinetic effects and their sample requirements (Note: optical methods, such as laser scattering light microscopy, are neglected here because they are only considered for particularly highly dilute dispersions (<< 1 vol.%) and small particle sizes (< 0.1 µm) and are thus generally unsuitable for EDL characterization of solid rocks.)

Thus, of the methods described in the literature, per se only the so-called streaming potential measurement is suitable for EDL characterization of solid rocks [34, 35]. However, this measurement has a significant disadvantage related to the systematic investigation of the EDL influence on the IP effect: the measurement on a solid rock sample provides only one value of the zeta

potential integrated over the entire sample volume, i.e., over all solid phase dependencies (table 1, left hand side). Thus, on the other hand, the systematic variations of the fluid dependencies (table 1, right hand side) lose significance or solely deliver basic descriptions of the EDL properties of the entire sample. Any other measurement technique for the determination of EDL parameters require particles in a dispersion medium, i.e., the "classical" colloidal systems as mentioned above.

Table 2. Overview of the main techniques for measuring electrokinetic effects.

electrical induced			
technique	**measured effect**	**sample type**	**particle size**
electrophoresis	electrophoretic mobility	colloidal	< 2 µm
electro-osmosis	electro-osmotic flow	colloidal	< 2 µm
electro-acoustic	electrokinetic sonic amplitude	colloidal	< 10 - 50 µm
mechanical induced			
technique	**measured effect**	**sample type**	**particle size**
sedimentation	sedimentation potential	colloidal	< 6,3 µm
fluid flow	streaming potential	solid	< 1 mm
acousto-electric	colloidal vibration potential	colloidal	< 200 - 300 µm

Of these methods, only electro-acoustic methods [41] thereby cover approximately the grain size range (particle size range) of a natural sedimentary rock [42]. Accordingly, this seems favourable in terms of the fundamental understanding of the IP-effect occurring at the solid-liquid-interface. In electroacoustic methods, the zeta potential is determined in two ways [36]: via the so-called "electrokinetic sonic amplitude effect" (ESA) and via the measurement of the so-called "colloid vibration potential" (CVP). The instrument available for this study uses the ESA measurement to determine the EDL parameters. Hence, this method is briefly described in the following. Figure 3 schematically shows the setup of the instrument. While the suspension is in continuous circulation in the system, an alternating voltage is applied between two plate electrodes (Fig. 3, D), which are in direct contact with the suspension. As the suspension passes through the alternating electric field, the dispersed particles are deflected toward the plates. This produces a measurable ultrasonic wave as all particles move in phase with each other. The ESA wave is decoupled by a silicate glass window (Fig. 3, B) and its amplitude converted into a signal by a piezoelectric transducer.

The ESA signal depends on the particle velocity and thus consequently on the particle charge and particle size. Larger particles are inert compared to small particles, causing a time delay between the change in direction of the electric field and the direction of particle motion (i.e., a change in sign of the particle velocity). By measuring the magnitude and phase of the ESA signal, both the zeta potential and the particle size can be determined [42]. The main advantage of the ESA method is that significantly larger particle (grain) sizes can be included for systematic investigations of natural rocks. Whereas classical methods are strictly limited regarding this parameter, ESA is able to include grains as large as up to 200-300 µm in diameter (i.e., at least 100 times larger grains than electrophoresis).

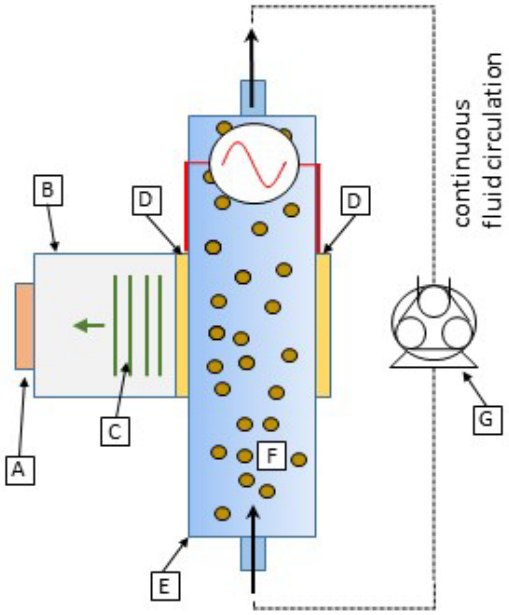

Fig. 3. Schematic illustration of the method used to measure the so-called electro-kinetic sound amplitude effect. (A) Piezoelectric transducer, (B) high-purity silicate glass, (C) ESA shaft, (D) plate electrodes, (E) measuring cell, (F) suspension, (G) peristaltic metering pump.

3 Sample preparation

At this point, it is obvious that a solid rock has to be turned back into an "unconsolidated material" if one wants to consider all relevant dependencies for EDL characterization (after completion of all further petrophysical, mineralogical, structural and topological investigations, of course). For the purpose of this new workflow, two different ways of doing this (the conventional, as well as the new approach) are presented in the following.

3.1 Conventional approach

The established standard procedure of sample crushing for (e.g.) geochemical analysis is to crush and grind up the material. However, not only are the mineral grains mechanically destroyed, but their surfaces in particular are transformed into an amorphous equivalent of themselves as the degree of grinding increases, i.e., as a result of greater pressure and rising temperature (Fig. 4). Chemically, the material does not change, but its surface and interfacial properties change, sometimes significantly, as a result, making it much more difficult to measure electrokinetic in-situ effects [34].

Furthermore, grinding destroys the original grain size distribution and creates a mono-modal grain size over time that does not exist in the original sample. Conclusively, mechanical crushing, milling and grinding of the material is (for obvious reasons) unsuitable to take the “in-situ” geometry and topology of the individual mineral grains of a clastic sedimentary rock during EDL characterization into account.

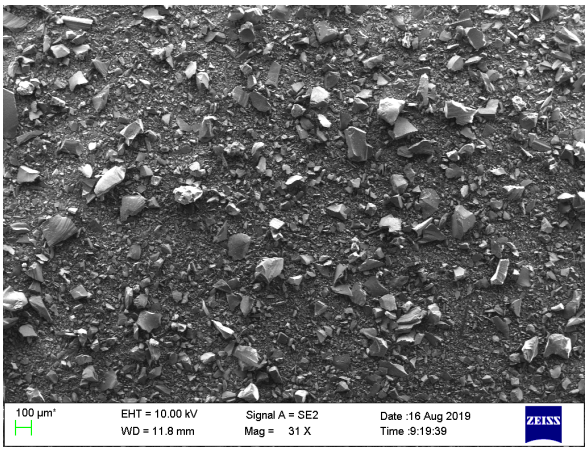

Fig. 4. SEM image showing the influence of conventional comminution (grinding) on the surface of quartz (originating from a Bentheimer sandstone). Clearly visible, sharp-edged fragments and mechanically destroyed surfaces that do not exist in the in-situ sample.

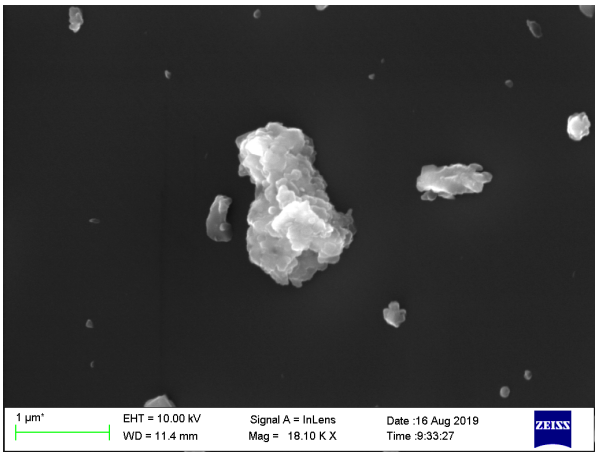

Fig. 5. SEM image showing that with increasing degree of comminution, the quartz surfaces are transformed by pressure and temperature into an amorphous equivalent (increasing "bubble formation" on the surface, grinding time 10 sec).

At this point, we would like to summarize the main issues, regarding the IP-related research of elektrokinetic properties, shortly:

- For a deeper understanding of the IP-effect of silici-clastic rocks, unravelling the electrokinetics of the material is essential.
- For this purpose, we need to investigate the sample material as closely to its in-situ stage as possible. Both, solid, as well as fluid parameter, need to be taken into account.
- Classical methods for electrokinetic measurements allow systematic variations of the fluid properties, but are measured either in a volumetric state of the sample or have to be performed on a colloidal system (rock-fluid suspension). Accordingly, solid phase dependencies cannot be investigated, or are at least greatly falsified by amorphous phase transitions during the preparation process.

3.2 Advanced disaggregation technique

After extensive research, the so-called "electrodynamic disaggregation technique" was identified as a suitable method and is described amongst others in [43, 44]. This method allows the fragmentation of rocks, mineral agglomerates, mono-mineral crystals and glasses along grain boundaries or internal material discontinuities (e.g., fluid inclusions, structures caused by dissolution, etc.). In this process, an electrical discharge is directed towards a non- or low-conductive material (rock) while it is immersed in a dielectric fluid (e.g., water or oil). In general, the electrical resistance of a solid phase is greater than that of a liquid phase.

However, this physical behavior changes radically as soon as the applied electrical voltage becomes very large and is released in the form of short pulses. Under these conditions, the rock behaves as a "conductor" and the liquid as an "insulator," with the sample acting as a "discharge channel" between the cathode and anode of the fragmentation apparatus [43]. Thus, large amounts of energy are accumulated along the sample axis, generating pressures similar to those of an explosion or a low-energy plasma discharge (up to 10^{10} Pa, [45]). The resulting pressure wave refracts along grain boundaries or along grain surfaces, inducing tensile stresses that lead to disaggregation of the rock sample. Figure 6 shows a principle drawing as well as the originally used apparatus.

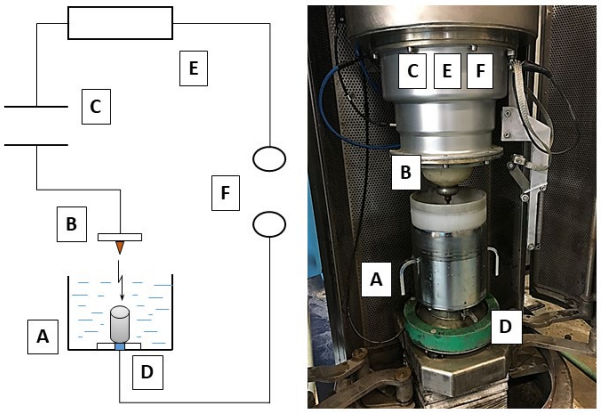

Fig.6. Schematic (left) and original (right) illustration of the setup and principle of the selFrag apparatus used to fragment the sandstone samples. (A) Water-filled sample collector, (B) cathode, (C) plate capacitor, (D) anode and rock sample, (E) resistor, (F) toggle switch.

3.3 Approval of disaggregation results

The fragmentation grade and the degree of preservation of the mineral grains of sandstones fragmented by this advanced sample disaggregation technique, was the subject of a preliminary study. In total, 30 samples (cylindrical plugs with a diameter of 30 mm and a length of 40 mm) of three different sandstones (Bentheimer - BE, Obernkirchen - OK, and Flechtingen - FL), with widely differing structural and physical properties, were fragmented in the processing laboratory of the leading company for this technique (selFrag).

The optimal, i.e., device and sample-specific fragmentation parameters, individually for each sandstone type, were systematically determined (Table 3). Following this work, the now processed and unconsolidated material was dried and further evaluated. Using scanning electron microscopy (SEM) and laser diffraction, the overall quality, degree of preservation and grain size distributions for each sample are assessed.

Table 3. Summary of optimal, unit-specific fragmentation parameters for each fragmented sandstone type.

rock	general sample characteristics	gap [mm]*	f [Hz]	U [kV]	pulses
BE	↓ clay; ↓↓ Fe; ↓↓ cement; ↑↑ Φ; ↑↑ k	40	5	150	10
OK	↓ clay; ↓↓ Fe; ↑ cement; ↑ Φ; ↓ k	40	5	150	30
FL	↑↑ clay; ↑ Fe; ↑↑ cement; ↓ Φ; ↓↓ k	35	5	150	40

*gap = distance cathode-sample;
↓↓ = very minor/low; ↓ = minor/low; ↑ = medium; ↑↑ = high.

Figure 7 shows an example of a Bentheim sandstone sample with a scanning electron micrograph before (Fig. 7, A) and after (Fig. 7, B) the fragmentation process. The significantly better degree of preservation of the individual mineral grains compared to grinding (see Fig. 4 & 5) is clearly noticeable. These are completely preserved in size and shape (Fig. 7B), as can be seen in direct comparison with the initial state (Fig. 7A). A temperature and pressure induced amorphous transformation of the grain surfaces is also not recognizable. Afterwards, the fragmented material was examined by laser diffraction with respect to its grain size distribution.

The result is shown in Figure 8. It can be clearly seen that the Bentheimer sandstone has a good sorting, i.e., a relatively narrow distribution of grain sizes. This distribution is dominated by grain sizes in the range 100 – 350 µm in diameter (about 90 % of all grains), which essentially reflects the matrix-forming mineral particles (primarily quartz and little feldspar). Grains smaller than 63 µm account for roughly 2 mass-% of all grain fractions of this sample, which is about 45 times less than the dominant size fraction.

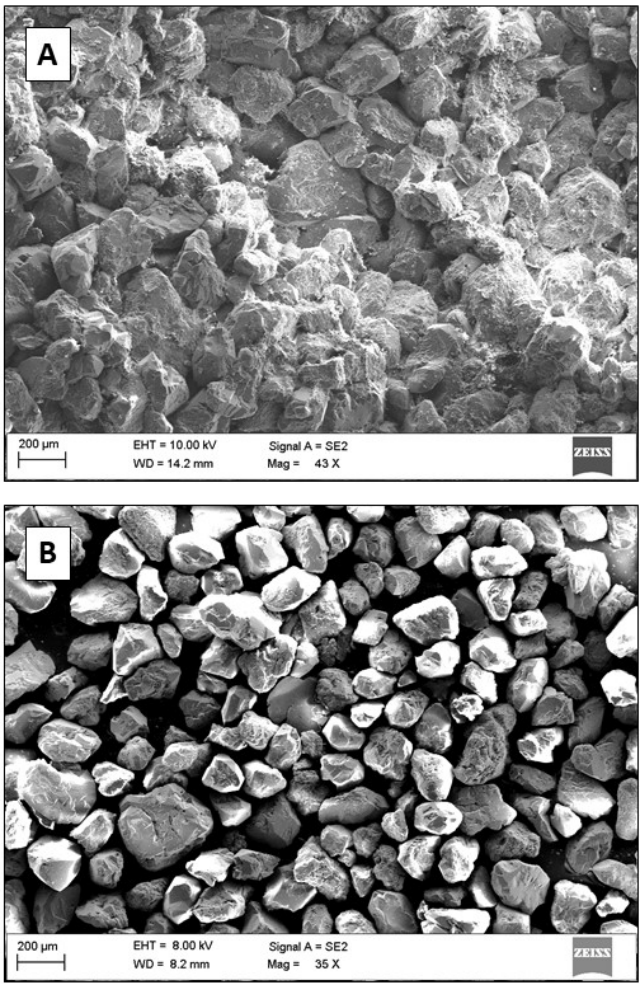

Fig. 7. Scanning electron image of a Bentheimer sandstone, before (A) and after (B) fragmentation using the selFrag apparatus. The excellent degree of preservation of the mineral grains is clearly visible (please note: minor components < 63 µm such as clay minerals and cement have been separated for the SEM analysis).

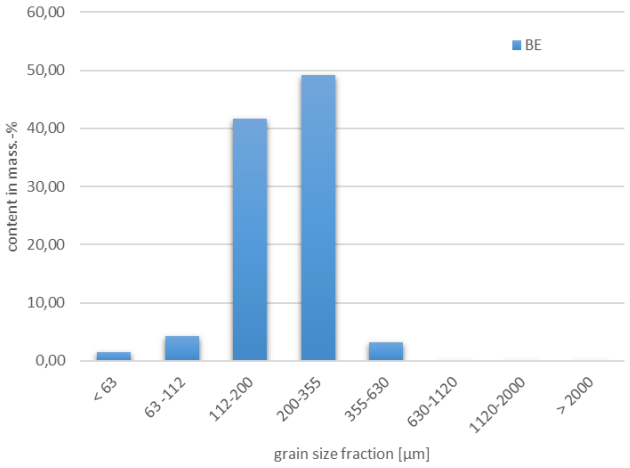

Fig. 8. Grain size distribution of the disaggregated Bentheimer sandstone sample (avg. of 10 samples).

4 Results

4.1 Petrophysics and SIP results

In advance to the disaggregation of the specimen, standard core analysis, as well as SIP-measurements have been conducted in order to characterize the different sandstones in terms of their basic petrophysical characteristics. Core analysis (here: grain density, porosity, permeability) followed protocols as referenced in [API RP40] and results are compiled in table 4. Results are presented for three different sandstones, originating from northern Germany: Bentheimer (BE), Obernkirchen (OK) and Flechtingen (FL) sandstone. As shown, the BE samples are characterized by an average porosity of 21 %, an average grain density of 2.65 g/cm³, and an average permeability of 575 mD, overall a "typical" cretaceous reservoir rock. The OK samples feature lower porosity (avg. 16.6 %) and permeability (avg. 19 mD), and slightly increased grain density due to the occurrence of carbonate cement within. FL samples feature lowest porosity (avg. 10.9 %) and permeability (avg. 6.2 mD), but also the highest average grain density due to the existence of Fe-oxides and a mixture of barite and carbonate cement within.

Table 4. Basic petrophysical properties of the investigated sandstones.

rock	porosity [%]			permeability [mD]		
	min	max	avg.	min.	max.	avg.
BE	20.2	22.2	21	529	653	575
OK	15.5	17.2	16.6	9	28	19
FL	6.5	16.6	10.9	0.3	32	6.2

For the SIP-measurements, samples have been saturated with a sodium-chloride solution, equivalent to an electrical conductivity of 100 mS/m (approx. 8 mmol/l NaCl). Measurements have been performed with a SIP-Quad device from Radic Research (Berlin, Germany) within a frequency range of 2 mHz to 10 kHz. For the SIP, averaged results of the quadrature conductivity (which is directly considered as a measure for the "IP-effect", compare section 1) over the investigated frequency range are presented for each rock type (Figure 9).

Each curve represents the averaged signal of ten individual SIP-measurements. Though all three sandstone types show local maxima of quadrature conductivity at frequencies between 0.01 and 1 Hz, differences are clearly visible. The BE samples feature the smallest amplitude maximum (barely 0.06 mS/m), almost doubled by the OK samples (0.12 mS/m), whereas the FL sandstone indicates the highest amplitude maximum (almost 0.28 mS/m). Both, BE and OK samples indicate their maximum at more or less the same frequency (~ 0.25 – 0.3 Hz). For FL, the maximum conductivity values are located one order of magnitude in frequency below BE and OK (~ 0.03 Hz).

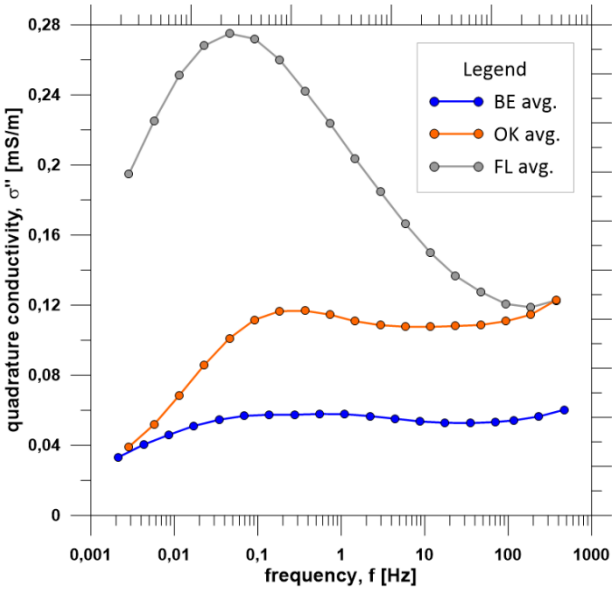

Fig. 9. Averaged results of the quadrature conductivity of the three investigated sandstones derived from SIP-measurements (top to bottom: Flechtingen - FL, Obernkirchen - OK, Bentheimer - BE).

4.2 Disaggregation results

Besides the already presented results for the Bentheimer sandstone (Fig. 7 & 8), SEM images and according grain size distributions for the OK and FL sandstones are presented.

Figure 10 shows a representative SEM image for the OK samples, showing a very good degree of preservation in terms of grain size and shape. The average grain sizes are smaller than for the BE samples. Nevertheless, some grains are still clearly cemented (Fig. 10, top right hand side), leading to larger, i.e., apparent grain sizes (Fig. 10, bottom) of 600 µm to > 2 mm. About 12 – 14 mass-% of the investigated sample material is affected. OK samples feature slight amount of carbonate cement, whereas BE samples are not cemented at all. This cement prevents a fragmentation of the OK samples as good as for the BE specimen. These grains have been sieved and removed for the ESA experiments. They are utilized for further investigation and optimization of the fragmentation process, respectively. Furthermore, OK sandstone features more grains < 63 µm than the BE type. This is in good accordance to the known mineralogy of both rocks, since the OK type features a higher content of clay minerals than the BE sandstone.

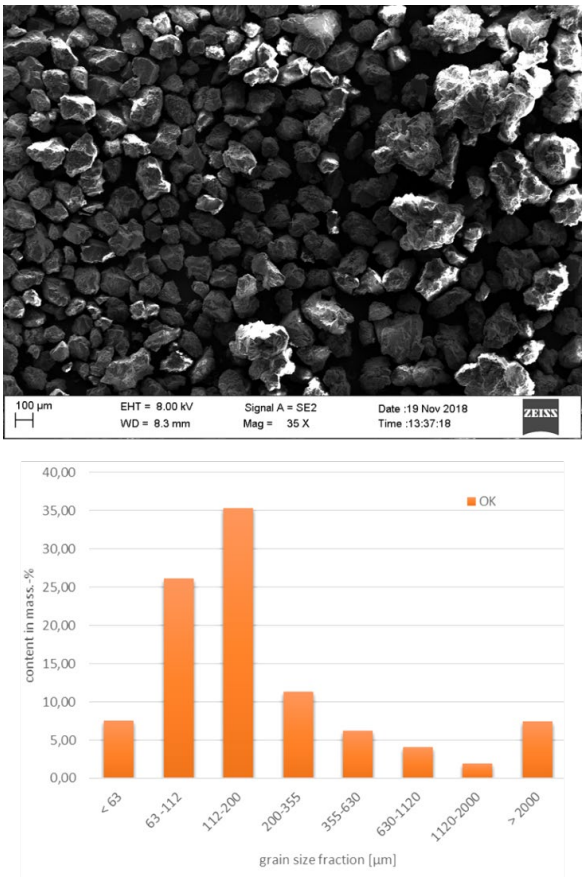

Fig. 10. Scanning electron image of the Obernkirchen sandstone (please note: minor components < 63 µm such as clay minerals and cement have been separated for the SEM analysis) after fragmentation using the selFrag apparatus (top), and the according grain size distribution (bottom, avg. of 10 samples).

Figure 11 shows the results from disaggregation and grain size analysis for the FL samples. Again, a very good degree of grain preservation is observed. The average grain size is higher than for OK, but in range with the BE sandstone. Nevertheless, the overall width of the distribution is significantly larger than for the BE type. Again, still cemented grains exist (sizes > 600 µm), caused by insufficient fragmentation, as for the OK samples. The slight, left-skewed distribution may indicate a slightly better fragmentation of the barite cement within the FL specimen compared to the carbonate cement of the OK samples. As before, these grains have been sieved and removed for the ESA experiments.

Furthermore, FL sandstone features more grains < 63 µm than the BE type, but little less than OK. It is known from extensive mineralogical investigations on the FL samples that they do feature a distinct amount of clay minerals within (smectite), which is distributed as “coating” upon the larger quartz grains. This coating has been partially broken during the fragmentation, accumulating in this grain size region. Additionally, FL specimens contain hematite (up to 5 vol.-%) with typical sizes in range of 20 – 35 microns. Accordingly, grains < 63µm are a mixture of broken smectite and hematite for the FL sandstone.

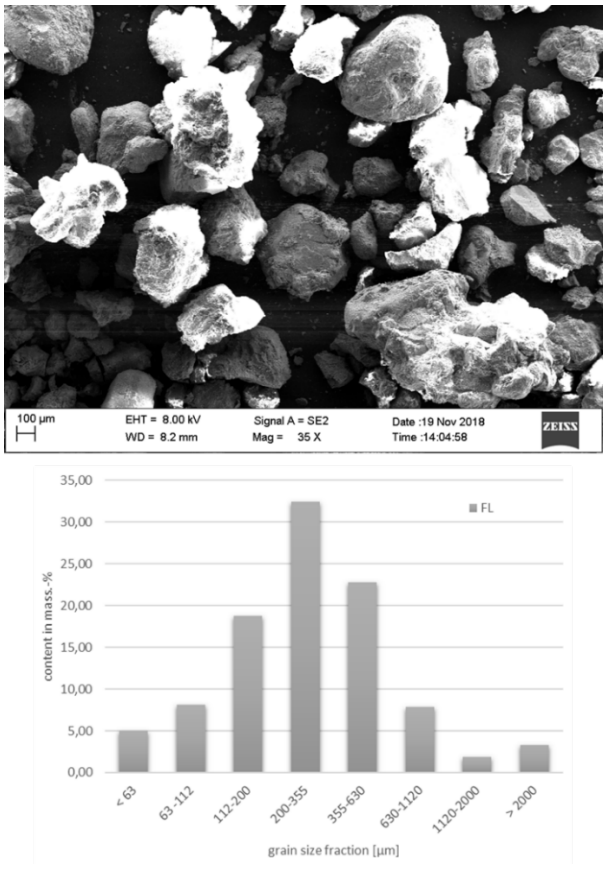

Fig. 11. Scanning electron image of the Flechtingen sandstone (please note: minor components < 63 µm such as clay minerals and cement have been separated for the SEM analysis) after fragmentation using the selFrag apparatus (top), and the according grain size distribution (bottom, avg. of 10 samples).

4.3 Zeta potential results

The zeta potential measurements have been conducted on suspensions, consisting of 5 mass-% of the fragmented sample material and 95 mass-% of sodium chloride solution, acting as carrier medium. For each sample, two different grain size fractions have been prepared: 2µm and 63-100µm. Additionally, a pure quartz crystal was milled and separated into a 2µm and 2-20µm grain size cluster, to highlight the influence of the sample preparation upon measured results. Figure 12 highlights the results for these experiments.

As it can be seen, zeta potential values for the 63-100µm fraction for both BE and OK samples is more or less in the same range, averaging to –2.75 mV. This size fraction is dominated by idiomorphic quartz and minor content of feldspar, which both form the main components of the rock matrix. In contrast, the according FL fraction clusters at lower zeta potential values, averaging to -23 mV. Though the matrix also mainly consists of quartz, grains are distinctively coated with smectite, causing this effect. For the smallest size fraction (2µm), BE zeta potential averages to -10 mV, OK to -15 mV, still close to each other, but visually separated from each other.

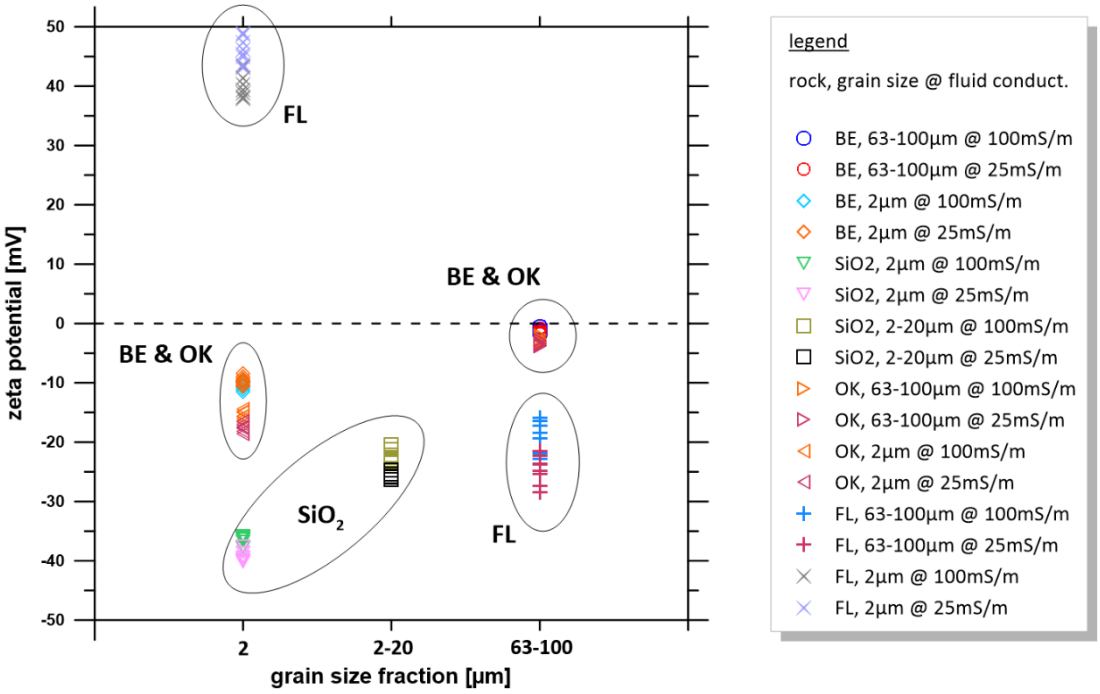

Fig. 12. Zeta potential versus selected grain size fractions for the three fragmented sandstones and a conventionally milled SiO_2 crystal.

In this grain size fraction, almost no quartz exist. Instead, this fraction is dominated by small clay mineral particles (mostly kaolinite and little illite), featuring a significantly larger surface area and electrokinetic potential. The separation indicates the difference in the clay types in between both samples: BE solely features kaolinite whereas OK inhibits a mixture of kaolinite and illite. For FL however, zeta potential values have turned into positive values for the 2µm grain size fraction, averaging to +43 mV. From mineralogical investigations, we know that parts of the smectite coating, originating from the large quartz grains, disaggregated into smaller pieces during fragmentation. However, smectite would lead to even larger negative zeta potentials than kaolinite and illite. According to our analysis, this result is caused by hematite, which originally exist as a fine dispersed phase within the Flechtingen sandstone. As Fe-oxide, hematite inhibits a very large and positive electro-kinetic potential, causing the observed effect.

The crushed and grinded SiO2 indicates a significant increase of the zeta potential with decreasing grain sizes. As described in section 3.1, grinding and milling leads towards an amorphous phase transition of the SiO2. Though the surface area increases compared to an idiomorphic crystal, this increase would not be sufficient to accumulate such a large electrokinetic potential. In fact, the "steepness" of the zeta potential increase for idiomorphic quartz is significantly smaller. However, the amorphous surface is able to "bind" more ions compared to the idiomorphic surface. This effect is described as an "apparent zeta potential" [46]. Here, it averages between -25 mV (for the 2-20 µm size fraction) and -37.5 mV (for the 2 µm fraction). These values are close to pure kaolinite and illite [33, 46, 47] and might lead to falsified interpretations in terms of pore scale interface processes and mineralogical composition.

4.4 Joint interpretation: ESA and SIP data

The results of the ESA measurements are in very good accordance compared to the SIP data. The BE samples feature less amount of clay minerals and cementation, hence the SIP signal amplitude is less pronounced than for the other sandstones. This context is also clearly visible within the zeta potential data. For large and (more or less) pure, idiomorphic quartz grains of the rock matrix, zeta potential values are small or even close to zero. The OK samples clearly indicate the exact same behaviour for the 63-100µm size fraction. Since the OK sandstone features slightly more clay minerals (both, mineral type and volume content), zeta potential values are more pronounced than for the BE specimens. This is in very good accordance to the literature from which is known that kaolinite features the lowest zeta potentials, followed by illite and smectites. The almost doubled SIP signal maximum of OK compared to BE can be directly related to this change in clay volume and mineralogy.

The FL samples feature the highest SIP signal amplitude, as a direct result of the highly polarizable hematite grains, possibly acting as small capacitors upon the surface of the rock matrix. The existence of smectite coatings upon the grain matrix is clearly verified by the distinctively higher (= more negative) zeta potential values for the 63-100µm fraction. Accordingly, the increased polarizability of smectite amplifies the effect of the hematite upon the main surfaces. As a matter of fact we can assume that two polarization mechanisms exist for this type of sandstone: an electronically conductance mechanism for the Fe-oxides and a classical ohmic surface conductance mechanism for the smectites.

5 Conclusions

The presented innovative techniques for highly controlled rock sample fragmentation (the so-called electrodynamic disaggregation technique) and zeta potential measurements are key for the advanced understanding of processes and for fundamental research at the solid-liquid interface of natural (reservoir) rocks. It is possible to link mineralogy, core and special core analysis (SIP), and electrokinetic properties directly, enhancing joint data interpretation and mechanistic model assumptions derived on larger scales. The appraisal and assessment of characteristic length scales (grain sizes) for these mechanisms has now become possible for the first time in SIP-related research. Nevertheless, two drawbacks exist: first, heavily cemented parts of the rock might not fragment as good as less cemented volumes, and might falsify the interpretation of grain size fractions (if not removed in advance). Second, non-clastic materials, i.e., biogenic carbonates, or any other rock without any distinct grain edges within, are most likely not able to be processed by this workflow. For this, carbonates and very fine-grained rock types (clay- and mudstones) are part of the ongoing research.

Acknowledgements

The authors would like to thank Daniel Parvaz from selFrag (Kerzers, Switzerland) for the support and fruitful discussions about the disaggregation technique. In addition, we would like to thank Prof. Dr. Helge Stanjek (RWTH Aachen, Germany) for his knowledge and time for discussing the ESA results, as well as Prof. Dr. Andreas Weller (TU Clausthal, Germany) for discussing the IP-effect theory.

References

1. W.K. Sawyer, C.I. Pierce, and R.B. Lowe, Petrophysics, **42**, 71-82 (2001).
2. D.P. Lesmes, and S.P. Friedman, **i**n: Y. Rubin, and S.S. Hubbard, Hydrogeophysics, Springer Publishing (2005).
3. J.B.T. Scott, and R.D. Barker, Quarterly Journal of Engineering Geology & Hydrogeology, **38**, 143-154 (2005).
4. A. Hördt, R. Blaschek, A. Kemna, and N. Zisser, Journal of Applied Geophysics, **62**, 33-46 (2007).
5. A. Weller, and L. Slater, Geophysics, **77** (5), 185-198 (2012), https://doi:10.1190/geo2012-0030.1.
6. Z. Zhang, and A. Weller, Geophysics, **79** (6), 377-387 (2014), https://doi:10.1190/geo2014-0143.1.
7. A. Weller, L. Slater, S. Nordsiek, and D. Ntarlagiannis, Geophysics, **75** (4), 105-112 (2010), https://doi:10.1190/1.3471577.
8. A. Weller, L. Slater, and S. Nordsiek, Geophysics, **78**, 315-325 (2013), https://doi:10.1190/geo2013-0076.1.
9. C. Weber, M. Halisch, and H. Stanjek, Clays and Clay Minerals, **66** (1), 86-95 (2018).
10. K. Titov, V. Tarasov, and A. Levitski, Journal of Applied Geophysics, **50**, 417-433 (2002).
11. L. Slater, and D.R. Glaser, Geophysics, **68**, 1547-1558 (2003).
12. A. Revil, and N. Florsch, Geophysical Journal International, **181**, 1480-1498 (2010), https://doi:10.1111/j.1365-246X.2010.04573.x.
13. K. Koch, A. Revil, and K. Hollinger, Geophysical Journal International, **190**, 230-242 (2012), https://doi:10.1111/j.1365-246X2012.05510.x.
14. J.B.T. Scott, and R.D. Barker, Geophysical Research Letters, **30**, 1450 ff. (2003).
15. S. Kruschwitz, A. Binley, D. Lesmes, and A. Elshenawy, Geophysics, **75**, 113-123 (2010), https://doi:10.1190/1.3479835.
16. K. Titov, A. Tarasov, Y. Ilyin, N. Seleznev, and A. Boyd, Geophysical Journal International, **180**, 1095-1106 (2010), https://doi:10.1111/j.1365-246X.2009.04465.x.
17. Q. Niu, and A. Revil, Geophysics, **81**, 17-32 (2016), https://doi:10.1190/GEO2015-0072.1.
18. H. Militzer, and F. Weber, Angewandte Geophysik, Bd.2, Springer Publishing (1985).
19. J. Schön, Petrophysik, Ferdinand Enke Publishing (1983).
20. G.E. Archie, Transactions of the American Institute of Metallurgists and Petroleum Engineers, **146**, 54-62 (1942), https://doi:10.2118/942054-G.
21. J.R. Schopper, in: G. Angenheister, Landolt-Börnstein, Bd.1b/V, Springer Publishing (1982).
22. J. Kuhlenkampff, and J.R. Schopper, in: SPWLA Transactions, Eleventh European Formation Evaluation Symposium (1988).
23. D.J. Marshall, and T.R. Madden, Geophysics, **24**, 790-816 (1959).
24. A. Blaschek, and A. Hördt, Near Surface Geophysics, **55**, 579-588 (2009).
25. M. Bücker, and A. Hördt, Geophysics, **78**, 229-314 (2013a), https://doi:10.1190/geo2012-9548.1.
26. M. Bücker, and A. Hördt, Geophysical Journal International, **194**, 804-813 (2013b), https://doi:10.1193/gji/ggt136.
27. H. Stebner, M. Halisch, and A. Hördt, Near Surface Geophysics, **15**, 563-578 (2017), https://doi:10.3997/1873-0604.2017054.
28. A. Hördt, K. Bairlein, M. Bücker, and H. Stebner, Near Surface Geophysics, **15**, 579-592 (2017), https://doi:10.3997/1873-0604.2017053.
29. D.P. Leroy, A. Revil, A. Kemna, P. Coszena, and A. Ghorbani, Journal of Colloid and Interface Science, **321**, 103-117 (2008), https://doi:10.1016/j.jcis.2007.12.031.
30. A. Revil, and M. Skold, Geophysical Journal International, **187**, 813-824 (2011), https://doi:10.1111/j.1365-246X.2011.05181.x.
31. A. Revil, Water Resources Research, **48**, W02517 (2012), https://doi:10.101029/2011WR011260.
32. J. Lyklema, and M. Minor, Colloids and Surfaces A: Physicochemical and Engineering Aspects, **140**, 33-41 (1998).
33. K. Jasmund, and G. Lagaly, Tonminerale und Tone – Struktur, Eigenschaften, Anwendung und Einsatz in Industrie und Umwelt. Steinkopff Publishing (1993).
34. J. Lyklema, Fundamentals of Interface and Colloid Science, Vol. II – Solid-Liquid Interfaces. Academic Press (2011).
35. R.J. Hunter, Zeta Potential in Colloid Science - Principles and Applications. Academic Press (1981).
36. Th. Luxbacher, The Zeta Potential for Solid Phases Analysis. 1. Edition, A48IP010EN-A (2014).
37. B.J. Kirby, Micro- and Nanoscale Fluid Mechanics: Transport in Microfluidic Devices. Cambridge University Press (2010).
38. S.S. Dukhin, and B.V. Derjaghuin, **i**n: Surface and Colloid Science, **7** (7), WileyPublishing (1974).
39. S.Y. Kang, and A.S. Sangani, Journal of Colloid and Interface Science, **165**, 195-211 (1994), https://doi.org/10.1006/jcis.1994.1220
40. A.V. Delgado, F. Gonzalez-Caballero, R.J. Hunter, L.K. Koopal, and J. Lyklema, Journal of Colloid and Interface Science, **209**, 194-224 (2007).

41. F. Hinze, S. Ripperger, and M. Stintz, Chemie Ingenieur Technik, **72**, 322-332, Wiley Publishing (2000).
42. R.W. O'Brian, A. Jones, and W.N. Rowlands**,** Colloids and Surfaces A: Physicochemical and Engineering Aspects, **218** (1-3), 89-111 (2003), https://doi.org/10.1016/S0927-7757(02)00593-9.
43. U. Andres, J. Jirestig, and I. Timoshkin, Powder Technology, **104**, 37-49 (1999)
44. E. Gnos, D. Kurz, I. Leya, and U. Eggenberger, Proceedings, Goldschmidt Conference (2007).
45. N.S. Rudashevsky, B.E. Burakov, S.D. Lupal, O.A.R. Thalhammer, and B. Saini-Eidukat, Trans. Inst. Mining Metal, **104**, C25-C29 (1995).
46. H.C. Li, and P.L. De Bruyn**,** Surface Science, **5**, 203-220 (1966).
47. C.H. Hamann, and W. Vielstich, in : Elektrochemie II – Elektrodenprozesse, Angewandte Elektrochemie. Verlag Chemie (1981).